

# Dye-sensitized solar cells with 13% efficiency achieved through the molecular engineering of porphyrin sensitizers

Simon Mathew<sup>1†</sup>, Aswani Yella<sup>1†</sup>, Peng Gao<sup>1</sup>, Robin Humphry-Baker<sup>1</sup>, Basile F. E. Curchod<sup>2</sup>, Negar Ashari-Astani<sup>2</sup>, Ivano Tavernelli<sup>2</sup>, Ursula Rothlisberger<sup>2</sup>, Md. Khaja Nazeeruddin<sup>1\*</sup> and Michael Grätzel<sup>1\*</sup>

**Dye-sensitized solar cells have gained widespread attention in recent years because of their low production costs, ease of fabrication and tunable aesthetic features, such as colour and transparency. Here, we report a molecularly engineered porphyrin dye, coded SM315, which features the prototypical structure of a donor- $\pi$ -bridge-acceptor and both maximizes electrolyte compatibility and improves light-harvesting properties. Linear-response, time-dependent density functional theory was used to investigate the perturbations in the electronic structure that lead to improved light harvesting. Using SM315 with the cobalt(II/III) redox shuttle resulted in dye-sensitized solar cells that exhibit a high open-circuit voltage  $V_{OC}$  of 0.91 V, short-circuit current density  $J_{SC}$  of 18.1 mA cm<sup>-2</sup>, fill factor of 0.78 and a power conversion efficiency of 13%.**

**D**ye-sensitized solar cells (DSCs) are an attractive solar energy conversion technology because of their low production cost, ease of fabrication and tunable aesthetic features, such as colour and transparency<sup>1–4</sup>. Initial forms of this technology used ruthenium(II)-based dyes in conjunction with iodide-based electrolytes to achieve a certified solar-to-electric power conversion efficiency (PCE) of 11.9% under full sun illumination (AM 1.5G, 1,000 W m<sup>-2</sup>)<sup>5</sup>. Surpassing the 12% PCE threshold required a paradigm shift in the chemical components utilized within this photo-electrochemical device<sup>6</sup>.

A new generation of DSCs is based on a combination of light-harvesting donor- $\pi$ -acceptor (D- $\pi$ -A) dyes in conjunction with cobalt-based redox mediators<sup>6–9</sup>. The strong molar absorptivity of D- $\pi$ -A dyes enables the use of thin TiO<sub>2</sub> films, potentially reducing fabrication costs relative to ruthenium(II) sensitizers, with concomitant improvements in the open-circuit voltage  $V_{OC}$  when used with cobalt-based redox mediators. The synthetic flexibility of D- $\pi$ -A dyes has enabled the engineering of enhanced compatibility toward these alternative redox couples by introducing steric bulk into the donor component and  $\pi$ -system, minimizing the unfavourable recombination between the electrolyte and the TiO<sub>2</sub> surface<sup>6–9</sup>. By using these new light harvesters, DSCs have achieved a maximum PCE of 12.3% under full sun illumination, utilizing the tris(2,2'-bipyridyl)cobalt(II/III) ( $[\text{Co}(\text{bpy})_3]^{2+/3+}$ ) redox shuttle. However, to achieve this PCE, the light harvesting of the porphyrin dye YD2-o-C8 was supplemented by the organic co-sensitizer Y123 (ref. 6). This landmark result began a renaissance for the DSC, validating the combination of D- $\pi$ -A dyes and cobalt redox mediators as an effective strategy in developing high-efficiency DSCs<sup>10</sup>.

The development of single-molecule panchromatic D- $\pi$ -A sensitizers remains a molecular engineering challenge in efforts to improve the overall PCE of DSC devices. Until now, achieving a panchromatic light-harvesting response in DSCs has relied on

co-sensitization, energy-relay strategies or tandem device configurations<sup>6,11–21</sup>. Although gains in PCE are often realized through improved light harvesting utilizing these strategies, the fabrication and optimization of these devices can be laborious and technically challenging. The development of a single D- $\pi$ -A sensitizer with a panchromatic light response in a DSC remains a main objective in the realization of maximum PCEs with standard device fabrication protocols<sup>6,22</sup>.

Porphyrin-based D- $\pi$ -A dyes provide a highly flexible platform for the development of panchromatic sensitizers<sup>6,23,24</sup>. The porphyrin chromophore has intrinsically strong light absorption in the Soret and Q-bands, but there is a lack of significant absorption in the spectral region between these two features. Typical porphyrin D- $\pi$ -A sensitizers comprising dialkylamine or diarylamine donors, in conjunction with an ethynylbenzoic acid acceptor, yield dyes with a vivid green colour, bereft of absorption between 500–600 nm (refs 6,24–29). Despite the high efficiency of these dyes in DSCs, further improvements to light harvesting through the use of stronger acceptors remains relatively unexplored<sup>30,31</sup>. Studies unrelated to the DSC have demonstrated that integration of proquinoidal units into the porphyrin structure causes strong perturbations to the electronic structure of the macrocycle<sup>32–35</sup>. These perturbations in benzothiadiazole-porphyrin analogues result in improved light harvesting by broadening and redshifting absorbance of the Soret and Q-bands.

In this work, we reengineered the prototypical structure of D- $\pi$ -A porphyrins to simultaneously maximize cobalt-electrolyte compatibility and improve the light-harvesting properties. Functionalization of the porphyrin core with the bulky bis(2',4'-bis(hexyloxy)-[1,1'-biphenyl]-4-yl)amine<sup>36</sup> donor and a 4-ethynylbenzoic acid yielded the green dye SM371, which exhibited a slightly improved PCE of 12% compared to the previously reported YD2-o-C8 (11.9%)<sup>6</sup>. Incorporation of the proquinoidal benzothiadiazole (BTD) unit into this structure afforded the dye SM315, a

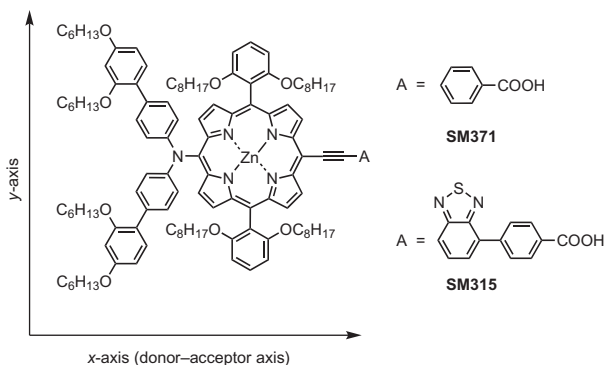
<sup>1</sup>Laboratory of Photonics and Interfaces (LPI), École Polytechnique Fédérale de Lausanne (EPFL), CH-1015, Lausanne, Switzerland, <sup>2</sup>Laboratory of Computational Chemistry and Biochemistry (LCBC), École Polytechnique Fédérale de Lausanne (EPFL), CH-1015 Lausanne, Switzerland; <sup>†</sup>These authors contributed equally to this work. \*e-mail: michael.gratzel@epfl.ch; mdkhaja.nazeeruddin@epfl.ch

1 panchromatic porphyrin sensitizer (Fig. 1). **SM315** exhibited significant broadening of Soret and Q-band absorbance features compared to **SM371**, yielding improved light harvesting in both the green (500–600 nm) and red (up to 800 nm) region of the spectrum. **SM315** demonstrated an enhancement in green light absorption, resulting in an improved  $J_{SC}$  (18.1 versus 15.9 mA cm<sup>-2</sup> for **SM315** and **SM371**, respectively) when utilized in the DSC. Ultimately, the panchromatic sensitizer **SM315** achieved a record 13.0% PCE at full sun illumination without the requirement of a co-sensitizer.

## Results and discussion

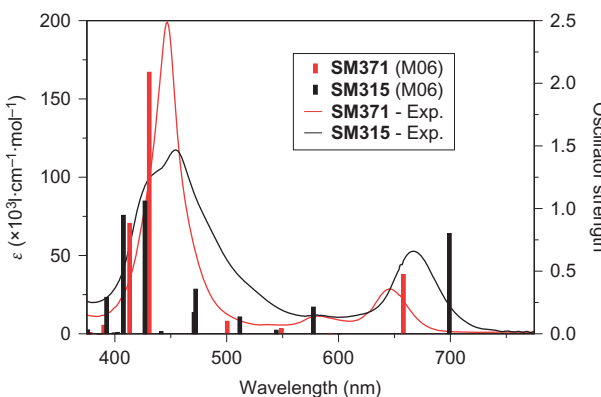
**Opto-electronic properties of the porphyrin sensitizers.** The syntheses of the dyes **SM371** and **SM315** are provided in the Supplementary Information. The donor group bis(2',4'-bis(hexyloxy)-[1,1'-biphenyl]-4-yl)amine was specifically used in the two dyes as it has demonstrated compatibility with cobalt-based electrolytes and yields high open-circuit photovoltages<sup>7,9,36</sup>. Table 1 summarizes the UV-vis, fluorescence and cyclic voltammetry data for **SM371** and **SM315**.

Figure 2 shows the solution (THF) absorption spectra of the **SM371** and **SM315** sensitizers. **SM371** features an absorption spectrum typical of porphyrins functionalized with a diarylamine donor and ethynylbenzoic acid acceptor, with maxima from the Soret band (B-band) at 447 nm and from the Q-bands at 580 nm and 646 nm. The introduction of the BTD acceptor unit had a significant impact



**Figure 1 | Structures of the two dyes used in the study.** The structures are coded **SM371** and **SM315**. They both feature a porphyrin core and a bulky bis(2',4'-bis(hexyloxy)-[1,1'-biphenyl]-4-yl)amine donor. Their acceptor groups differs, with **SM315** featuring a benzothiadiazole group.

on the absorption spectrum of **SM315**, most evident by the splitting of the Soret band, resulting in a shoulder at 440 nm on the maximum at 454 nm. Furthermore, the absorption of **SM315** between the Soret and Q-bands (450–550 nm) displayed significant enhancement compared to **SM371**, leading to the panchromatic character of the BTD-functionalized dye. The Q-band at 581 nm remained relatively constant compared to that of **SM371**, but the



**Figure 2 | Absorption spectra of the dyes studied.** The experimental spectra (in THF) are shown as continuous lines and the theoretical electronic transitions are shown as bars for both **SM371** (red) and **SM315** (black). Theoretical data were computed using LR-TDDFT/M06/IEF-PCM(THF).

lowest-energy Q-band absorption of **SM315** was significantly redshifted to 668 nm. Both the spectral splitting and the redshifting of absorbance maxima for **SM315** are consistent with previously reported porphyrin-BTD ensembles<sup>32,37</sup>.

The splitting of the Soret band in **SM315** can be rationalized using point-dipole exciton coupling theory<sup>37</sup>. The Soret band (B-band) is a composition of two perpendicularly polarized transitions within the molecule, denoted  $B_x$  and  $B_y$ , where the  $x$ -axis has the greatest degree of conjugation (that is, the donor–acceptor axis, Fig. 1)<sup>38,39</sup>. In a symmetrical zinc tetraphenylporphyrin the  $B_x$  and  $B_y$  transitions are degenerate. Functionalization of the porphyrin with donor and acceptor moieties to afford **SM371** increased the conjugation and charge transfer (CT) character along the donor–acceptor axis (that is,  $x$ -axis) of the dye, causing the Soret absorption originating from the  $B_x$  transition to be redshifted with increased molar absorptivity. Overall, the Soret band in **SM371** appears both broad and redshifted, as the  $B_x$  and  $B_y$  transitions are no longer degenerate. The presence of the BTD-functionalized acceptor in **SM315** further increased the electronic asymmetry and CT character of the dye, causing a redshifted  $B_x$  transition, which resulted in the Soret band appearing as two distinguishable maxima in the absorbance spectrum. Furthermore, the presence of the BTD acceptor increased the  $x$ -axis polarizability of **SM315**, indicative of increased oscillator strength for the  $B_x$  transition, rationalizing the differences in molar absorptivity between the two Soret maxima.

Another noticeable difference in the spectra of the two dyes is the redshift and increase in molar absorptivity of the lowest-energy Q-band for **SM315**. For both dyes, the absorbance originating from the  $Q_y$  transition remains relatively unperturbed, appearing at 580 nm and 581 nm in **SM315** and **SM371**, respectively. The increased conjugation along the  $x$ -axis of **SM315** strongly shifted absorbance from the  $Q_x$  transition to produce a maximum at 668 nm. The significant increase in molar absorption coefficient is consistent with the increased oscillator strength of the  $Q_x$  transition from enhanced  $x$ -axis polarizability within the **SM315** upon introduction of the BTD unit.

Comparison of the frontier Kohn–Sham (KS) orbitals between the two compounds highlighted the effect of the BTD acceptor on the electronic structure of **SM315** (Fig. 3). The KS highest occupied molecular orbital (HOMO) of both dyes was predominantly localized on the donor and was not affected by the choice of acceptor. The location of the KS lowest unoccupied molecular orbital (LUMO) in **SM315** demonstrated a significant shift towards the BTD component of the acceptor. Hence, the electronic transition

**Table 1 | Optical and electrochemical data for SM371 and SM315.**

Dye	$\lambda_{abs}$ (nm)/ $\epsilon$ ( $10^3$ M <sup>-1</sup> cm <sup>-1</sup> )	$\lambda_{em}$ (nm)*	$E_{0-0}$ (eV) <sup>†</sup>	$E_{ox1}$ (V)	$E_{red1}$ (V)
<b>SM371</b>	447/199, 580/12, 646/29	674	1.88	0.89	-1.21
<b>SM315</b>	440/105, 454/117, 581/12, 668/53	732	1.79	0.88	-0.99

\*Emission maxima obtained in THF by excitation at 440 nm.

<sup>†</sup>Zero-zero excitation energy, determined by the intersection of normalized absorbance and emission spectra.

in **SM315** with a dominant HOMO → LUMO contribution was expected to exhibit an enhanced CT character compared to **SM371**. The calculated absorption spectra for **SM371** and **SM315** (Fig. 2) were obtained by using linear-response time-dependent density functional theory (LR-TDDFT) and the M06 functional<sup>40</sup>. An integral equation formalism of the polarizable continuum model (IEF-PCM) with a relative permittivity of 7.43 was used to simulate the solvent (THF) used for the experimental absorption data (see Supplementary Information for full computational details and a discussion of the protocol used). The LR-TDDFT/M06/IEF-PCM(THF) methodology predicted a strong alteration of the Soret band for **SM315**, with two distinct transitions appearing at 408 nm and 427 nm (3.04 and 2.90 eV, respectively), with similar oscillator strengths, consistent with the splitting observed experimentally, which contributes to the panchromatic character of the dye. Analysis of the transition density difference plots (Supplementary Fig. 2) for the two Soret transitions of **SM315** revealed that the lower-energy Soret absorption exhibited a significant contribution from the BTD acceptor (that is, greater polarization along the donor–acceptor axis due to an enhanced CT character), consistent with the rationalization provided from point-dipole exciton coupling theory (*vide supra*). In contrast, the LR-TDDFT/M06/IEF-PCM(THF) absorption spectra of **SM371** indicated that the Soret band is dominated by a strong transition at 431 nm and a weaker second transition computed at 413 nm, reproducing the trends in Soret band splitting observed experimentally between the two dyes.

The calculated absorption of **SM315** presented a vertical transition with moderate oscillator strength (0.213) at 578 nm (2.15 eV), with significant donor-to-acceptor character (HOMO-1 → LUMO, 83%). This small absorption, in line with the experimental observation, also contributes to the enhanced panchromatic light-harvesting ability of **SM315**, together with a series of absorption lines between 601 nm and 430 nm. The calculated absorption spectra afforded a first vertical excitation at 658 nm (1.88 eV) and 699 nm (1.77 eV) for **SM371** and **SM315**, respectively, consistent with the experimental values of 646 nm (1.92 eV) and 668 nm (1.86 eV) for the lowest-energy Q-bands. For both dyes, this first

electronic transition is characterized by a dominant HOMO → LUMO contribution of comparable magnitude, 91% for **SM371** and 88% for **SM315**, confirming the CT character of both dyes (further supported by transition density plots; Supplementary Figs 1,2). The presence of the BTD moiety in **SM315** results in an extended delocalization of the LUMO onto this acceptor site, enhancing the CT character of this band, together with a shift towards lower energy and higher oscillator strength. The second transition is computed at a similar energy for both dyes, 600 nm (**SM315**) and 592 nm (**SM371**), and displays in both cases small oscillator strength and a similar character (Supplementary Figs 1 and 2).

Characterization of the surface-mounted dyes was achieved by adsorbing the sensitizer onto a 1-μm-thick TiO<sub>2</sub> substrate following acquisition of a Fourier transform infrared (FTIR) spectrum (Supplementary Fig. 3). On adsorption to TiO<sub>2</sub>, the FTIR spectra revealed the disappearance of the carbonyl stretch, ν(C=O), at 1,690 cm<sup>-1</sup> from the neat dye, with a concomitant increase in the intensity of the band at 1,380 cm<sup>-1</sup>, which originates from the symmetric carboxylate band, ν(COO<sub>sym</sub><sup>-</sup>). This change is characteristic of bidentate binding by both oxygen atoms of the carboxylate functional group to the titania of the substrate, consistent with previous reports<sup>41–43</sup>.

UV-vis characterization of the surface-mounted dyes was achieved by adsorbing the sensitizer onto a 1-μm-thick TiO<sub>2</sub> substrate (data presented in the Supplementary Information; Supplementary Fig. 4). Both dyes experienced a slight blueshift on adsorption to the titania, which was attributed to the decrease in dipole following loss of the carbonyl moiety of the anchoring group, consistent with observations from FTIR analysis of the substrate. The degrees of blueshift for absorptions derived from the *B*<sub>y</sub> and *Q*<sub>y</sub> transitions were less than for those derived from the *B*<sub>x</sub> and *Q*<sub>x</sub> transitions, consistent with the rationale provided by point-dipole exciton coupling theory (*vide supra*). Measurement of the light-harvesting efficiency (LHE) of **SM371** and **SM315** on transparent TiO<sub>2</sub> films (3.5 μm) is provided in the Supplementary Information (Supplementary Fig. 5). The LHEs for **SM371** and **SM315** exhibited maxima that correlated with those observed in

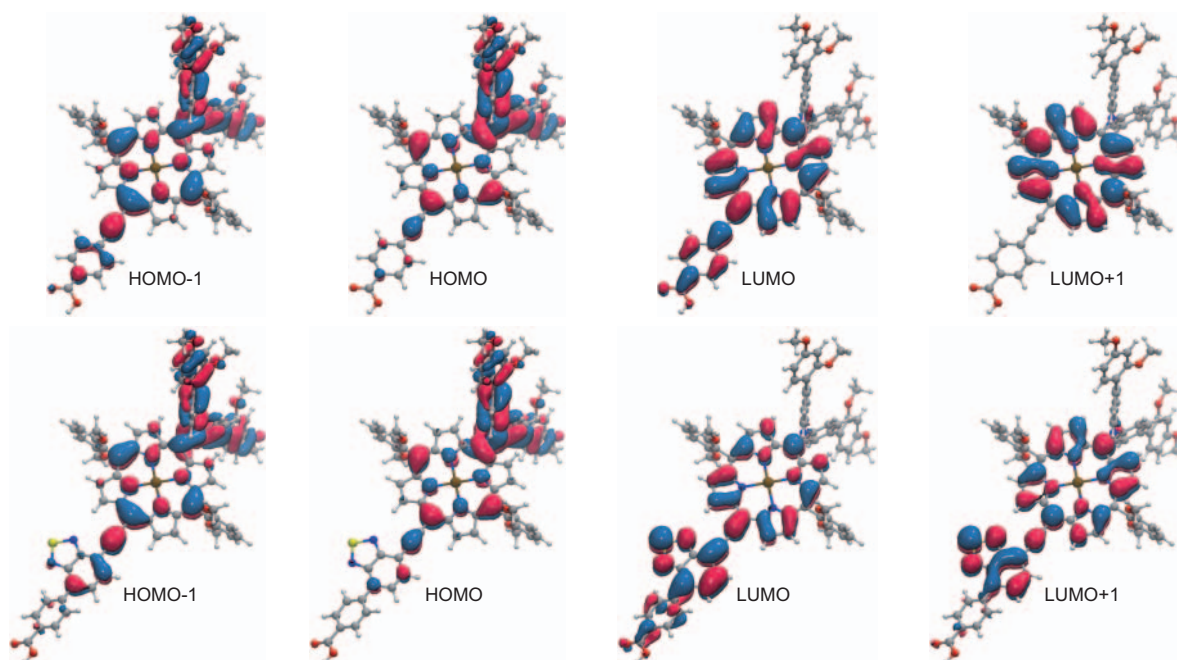


**Figure 3 | Contour plots of selected KS orbitals for the dyes studied.** The orbitals were calculated for geometry-optimized **SM371** (top) and **SM315** (bottom), using DFT/M06/IEF-PCM(THF). (Isovalue set to 0.02 a.u.)

Q10

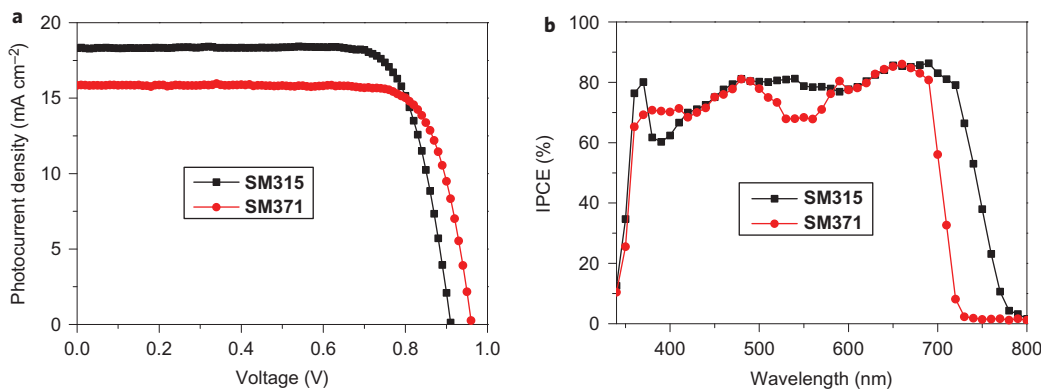


**Figure 4 | Photovoltaic performance of devices made with SM371 and SM315.** **a,b,**  $J$ - $V$  curve under AM 1.5G illumination ( $1,000 \text{ W m}^{-2}$ ) (**a**) and photocurrent action spectrum (**b**) for SM371 (red) and SM315 (black).

the experimental absorption spectrum. Measurement of LHE revealed that SM315 has a near-quantitative LHE throughout the visible region, which is a dramatic improvement over SM371. The splitting and redshifting of Soret and Q-band absorptions upon introduction of the BTD unit into the dye structure is directly responsible for the significant improvements in LHE demonstrated by SM315. The dye loading on the  $\text{TiO}_2$  films was obtained by desorbing the dyes, and the amount of dyes loaded was estimated to be  $8.35 \times 10^{-7} \text{ mol cm}^{-2}$  for the case of the SM315 dye. Assuming a uniform coverage on the titania without any aggregates, the SM315 dye occupies a surface area of  $\sim 1.98 \text{ nm}^2$  on the  $\text{TiO}_2$ .

The steady-state fluorescence spectra for SM371 and SM315 are provided in the Supplementary Information (Supplementary Fig. 6). SM371 exhibited an emission spectrum that mirrored the absorption spectrum, but that of SM315 was broad and featureless, indicating that an enhanced ICT character of the excited state could be achieved by using the strongly electron-deficient BTD unit, thereby increasing the acceptor property of the dye<sup>44</sup>. Calculation of the Stokes shift for the two dyes revealed that SM315 ( $1,309 \text{ cm}^{-1}$ ) experienced a greater shift than SM371 ( $643 \text{ cm}^{-1}$ ). The acquisition of time-resolved luminescence in THF solution and on  $\text{TiO}_2$  substrates provided insight into the electron injection dynamics of the two dyes (Supplementary Fig. 7). The fluorescence lifetime in solution (1.2 ns) and on  $\text{TiO}_2$  substrates (63 and 60 ps for SM371 and SM315, respectively) was identical for both dyes. This is indicative of the injection efficiency ( $\eta_{\text{inj}}$ ) for both dyes approaching unity, as a result of efficient photoinduced electron injection from the dye into the mesoporous anode.

**Electrochemical characterization.** The electrochemical characterization of SM371 and SM315 was performed in DMF. The oxidation potential of the dyes is critical for the functioning of the DSC, as it determines the optimal cobalt redox couple to be utilized within the cell. The first oxidation potentials of SM371 and SM315 were both quasi-reversible, with values of +0.88 V and +0.89 V (versus NHE), respectively. The computed vertical ionization energies (of the ground-state geometry) in DMF are nearly identical for both dyes (4.86 eV and 4.85 eV for SM371 and SM315, respectively), consistent with the trend observed in oxidation potential and the observation that the HOMO of SM315 is not strongly affected by the BTD moiety.

The reduction potentials of SM371 and SM315 were -1.21 V and -0.99 V (versus NHE), respectively. The similarity of  $E_{\text{ox}}$  for the two dyes demonstrated a considerable advantage of the BTD-functionalized anchor, as it does not noticeably impact the oxidation potential of the dye. The BTD-functionalized anchor exclusively influenced the optical bandgap and absorption features of SM315 (*vide supra*), allowing us to engineer the absorption features and

oxidation potential of the porphyrin in a separate, modular fashion. The difference in reduction potential demonstrated the ability of the BTD unit to stabilize the LUMO, consistent with the redshift observed in the absorption spectrum of SM315.

Further insight into the interfacial electron transfer (that is, from the photoexcited dye to the semiconducting photoanode) was performed by intensity-modulated photoinduced absorption (PIA) measurements on  $\text{TiO}_2$  films sensitized with SM371 and SM315 (Supplementary Fig. 8). Measuring the change in absorbance of the sensitized films in the absence of electrolyte (that is, acetonitrile solvent) revealed a decrease in absorbance from the Q-band, with concomitant evolution of an absorbance at 800 nm, diagnostic of formation of the porphyrin cation radical for both dyes<sup>28</sup>. Interestingly, the amount of dye cation radicals generated by SM315 in the absence of the electrolyte appears to be less than for SM371, indicating that the injected electron recombines with the photo-oxidized sensitizer faster for SM315 than for SM371. This back reaction is facilitated by the presence of the strongly electron-deficient BTD moiety in SM315 and is consistent with previous reports where the undesirable electron-recapture event could be partially ameliorated through the introduction of a phenyl spacer between the BTD and the anchoring group<sup>45</sup>. In the presence of the cobalt electrolyte, absorbance features pertaining to the porphyrin cation radical disappear entirely, indicating efficient regeneration of the porphyrins by the Co(II) species of the redox couple<sup>6</sup>.

**Photovoltaic performance.** Dyes SM371 and SM315 were utilized in DSCs using thin ( $7 \mu\text{m}$ ) mesoporous  $\text{TiO}_2$  films to enable compatibility with the  $[\text{Co}(\text{bpy})_3]^{2+/3+}$  redox couple, essential in obtaining DSCs exhibiting a high  $V_{\text{OC}}$ . Figure 4 shows the  $J$ - $V$  curve for the two devices measured under AM 1.5G illumination ( $1,000 \text{ W m}^{-2}$  at 298 K) (data summarized in Table 2). DSCs fabricated using SM371 gave a high  $V_{\text{OC}}$  (0.96 mV) and  $J_{\text{SC}}$  ( $15.9 \text{ mA cm}^{-2}$ ), achieving an overall PCE of 12.0%, a slight improvement compared to the porphyrin sensitizer YD2-o-C<sub>8</sub>, which has a similar structure<sup>6</sup>. Despite exhibiting a slightly lower  $V_{\text{OC}}$  of 0.91 V, the best cell made with SM315 attained a higher  $J_{\text{SC}}$  ( $18.1 \text{ mA cm}^{-2}$ ) and an overall PCE of 13.0%, outperforming SM371 as a result of the improvement in visible and near-infrared light harvesting. A histogram of 50 different devices made with

**Table 2 | Summary of photovoltaic performance data for SM371 and SM315 under AM 1.5G illumination ( $1,000 \text{ W m}^{-2}$ ).**

Dye	$V_{\text{OC}}$ (V)	$J_{\text{SC}}$ ( $\text{mA cm}^{-2}$ )	FF	PCE (%)
SM371	0.96	15.9	0.79	12.0
SM315	0.91	18.1	0.78	13.0

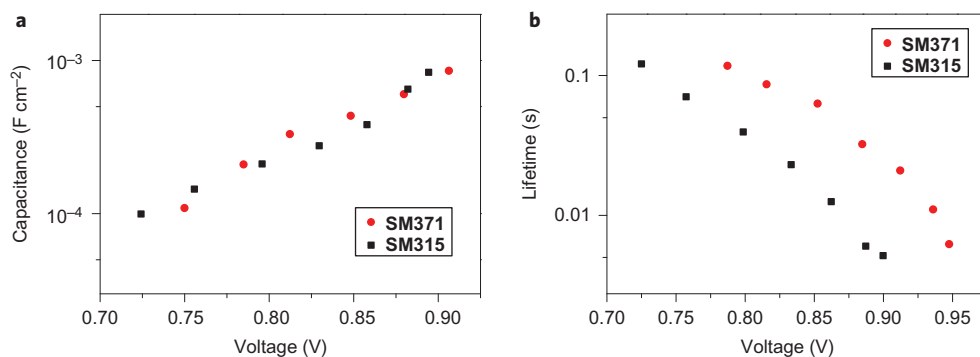


**Figure 5 | Transient photocurrent and photovoltage measurements carried out on devices made with SM315 and SM371. a,b,** Chemical capacitance (a) and electron lifetime (b) as a function of  $V_{OC}$  obtained through transient photocurrent and photovoltage measurements.

1 SM315 dye is shown in Supplementary Fig. 10. A higher average  
 2 PCE was obtained at 64% sun intensity (13.25%) than at full sun  
 3 intensity (12.75%). The lower average at full sun intensity is  
 4 mainly due to mass transport limitations of the cobalt  
 5 redox mediator.

6 SM371 possessed a near identical photocurrent action spectrum  
 7 (Fig. 4b) to that of dyes with comparable donor and acceptor sub-  
 8 stitution (that is, YD2-o-C8), with maximum IPCE values of 80%  
 9 obtained at 480, 590 and 640 nm. SM315 demonstrated impress-  
 10 ively high IPCE values across the whole visible wavelength range,  
 11 maintaining a value of 80% from 450 nm to 750 nm, with the  
 12 DSC harvesting light up to 800 nm, demonstrating the utility of  
 13 the BTD-functionalized anchor for visible and infrared light-har-  
 14 vesting properties. The overlap integral of the photocurrent action  
 15 spectrum with the standard AM 1.5G solar emission spectrum is  
 16 in excellent agreement (within 2%) with the measured photocur-  
 17 rent, demonstrating that any spectral mismatch between the simu-  
 18 lated and true AM 1.5G sunlight is negligibly small.

19 Transient photovoltage and photocurrent measurements were  
 20 used to investigate the origin of reduced  $V_{OC}$  for DSCs sensitized  
 21 with SM315. A reduction in  $V_{OC}$  can originate from either (1)  
 22 downward shift of the conduction band or (2) the enhanced recom-  
 23 bination of injected charges in the  $\text{TiO}_2$  film with the dye or electro-  
 24 lyte.<sup>46–48</sup> A downward shift of the  $\text{TiO}_2$  conduction band (that is,  
 25 displacement of the trap-state distribution function to lower  
 26 energy) would cause the density of occupied states (DOS) to be  
 27 higher for SM315 than for SM371.<sup>46–48</sup> Measurement of the  
 28 chemical capacitance ( $C_\mu$ , Fig. 5a) as a function of  $V_{OC}$  allows  
 29 insight into the DOS in devices made with either dye, as  $C_\mu$  and  
 30 DOS are directly proportional to each other. At a given  $V_{OC}$ ,  $C_\mu$   
 31 is nearly identical for both dyes, ruling out a downward shift of  
 32 the conduction band shift as the origin of the decreased  $V_{OC}$  in  
 33 SM315-sensitized DSCs.

34 Measurement of the electron lifetimes as a function of  $V_{OC}$   
 35 (Fig. 5b) afforded insight into the electron recombination occurring  
 36 at the  $\text{TiO}_2$ -electrolyte interface. At a given  $V_{OC}$ , the electron  
 37 lifetime in cells sensitized with SM371 was two to six times longer  
 38 than for SM315-sensitized DSCs. Evidence from previous work  
 39 clearly demonstrates that the direct connection of the BTD group  
 40 to the anchoring group accelerated conduction-band electron recap-  
 41 ture by the sensitizer and the utilization of a phenyl spacer retards the  
 42 electron recapture.<sup>45</sup> In this work, the PIA spectrum of SM315  
 43 (Supplementary Fig. 8b) clearly demonstrated that even with a  
 44 phenyl spacer in place, the electron recapture by SM315 is faster  
 45 than by SM371. This indicates that the phenyl spacer does not com-  
 46 pletely attenuate the accelerating effect of the BTD moiety on charge  
 47 carrier recombination (*vide supra*). The result of the accelerated  
 48 electron recapture by SM315 (compared to SM371) at the  $\text{TiO}_2$ -  
 49 electrolyte interface resulted in a  $V_{OC}$  decrease of 50 mV in the

device. However, this loss in  $V_{OC}$  is overcompensated by a gain in  $J_{SC}$  resulting in the superior performance of the SM371 dye.

Long-term stability measurements were carried out on three individual devices sensitized with SM315 by subjecting them to continuous light soaking at full solar light intensity for 500 h at 298 K (Supplementary Fig. 11). The cells were kept at their maximum power point during the illumination. We obtained excellent stability over this long period, showing that the SM315 is a very stable dye and not prone to degradation, even if exposed to intense sunlight for long illumination times. During the 500 h of light soaking, devices employing SM315 underwent over one million turnovers without showing any significant loss in stability. The initial drop in PCE of ~10–20% for the three devices is attributed to desorption of a small amount of sensitizer from the  $\text{TiO}_2$  surface, decreasing the photovoltaic performance. In the future, the introduction of stronger anchoring groups into the high-performance SM315-type design should serve to minimize any dye desorption and further improve the stability of the device.

## Conclusion

Judicious molecular engineering of push-pull porphyrins has allowed the realization of two high-performance sensitizers, SM371 and SM315, exhibiting unprecedented solar-to-electric PCEs under standard AM 1.5G illumination. The green dye SM371 exhibited slightly better performance (12.0%) than the previous state-of-the-art YD2-o-C8. Introduction of the BTD-functionalized acceptor into the dye structure afforded the broadly absorbing sensitizer SM315. The enhanced visible and long wavelength absorbance properties of SM315 were rationalized by LR-TDDFT analysis. The dramatically improved absorption properties of SM315 resulted in a near-quantitative LHE across the visible spectrum and up to 800 nm, leading to greater photocurrents in the DSC device compared to SM371. Fabrication of DSCs utilizing the  $[\text{Co}(\text{bpy})_3]^{2+/\text{3}+}$  redox couple and SM315 demonstrated panchromatic light harvesting without the use of co-sensitization, leading to a record 13% PCE at full sun illumination.

## Methods

Details of the synthesis and characterization of the dyes, computational investigations, DSC fabrication and photovoltaic characterization ( $J-V$ , IPCE, PIA, transient photovoltage/photocurrent decay, stability measurements) are described in the Supplementary Information.

Received 22 September 2013; accepted 20 December 2013;  
 published online XX XX 2014

## References

- O'Regan, B. & Grätzel, M. A low cost, high-efficiency solar cell based on dye-sensitized colloidal  $\text{TiO}_2$  films. *Nature* **353**, 737–740 (1991).

- 1 2. Grätzel, M. Conversion of sunlight to electric power by nanocrystalline  
2 dye-sensitized solar cells. *J. Photochem. Photobiol. A* **164**, 3–14 (2004).
- 3 3. Shah, A., Torres, P., Tscharner, R., Wyrtsch, N. & Keppner, H. Photovoltaic  
4 technology: the case for thin-film solar cells. *Science* **285**, 692–698 (1999).
- 5 4. Grätzel, M. Dye-sensitized solar cells. *J. Photochem. Photobiol. C* **4**, 145–153  
6 (2003).
- 7 5. Komiya, R. *et al.* Improvement of the conversion efficiency of a monolithic type  
8 dye-sensitized solar cell module. *Technical Digest, 21st International Photovoltaic  
9 Science and Engineering Conference*, Fukuoka, 2 C-5O-08 (2011).
- 10 6. Yella, A. *et al.* Porphyrin-sensitized solar cells with cobalt (II/III)-based redox  
11 electrolyte exceed 12 percent efficiency. *Science* **334**, 629–634 (2011).
- 12 7. Feldt, S. M. *et al.* Design of organic dyes and cobalt polypyridine redox  
13 mediators for high-efficiency dye-sensitized solar cells. *J. Am. Chem. Soc.* **132**,  
14 16714–16724 (2010).
- 15 8. Yum, J. H. *et al.* A cobalt complex redox shuttle for dye-sensitized solar cells with  
16 high open-circuit potentials. *Nature Commun.* **3**, 631 (2012).
- 17 9. Tsao, H. N. *et al.* Cyclopentadithiophene bridged donor–acceptor dyes achieve  
18 high power conversion efficiencies in dye-sensitized solar cells based on the tris-  
19 cobalt bipyridine redox couple. *ChemSusChem* **4**, 591–594 (2011).
- 20 10. Hardin, B. E., Snaith, H. J. & McGehee, M. D. The renaissance of dye-sensitized  
21 solar cells. *Nature Photon.* **6**, 162–169 (2012).
- 22 11. Ogura, R. Y. *et al.* High-performance dye-sensitized solar cell with a multiple dye  
23 system. *Appl. Phys. Lett.* **94**, 073308 (2009).
- 24 12. Wu, H. P. *et al.* Molecular engineering of cocktail co-sensitization for efficient  
25 panchromatic porphyrin-sensitized solar cells. *Energy Environ. Sci.* **5**,  
26 9843–9848 (2012).
- 27 13. Hardin, B. E. *et al.* Increased light harvesting in dye-sensitized solar cells with  
28 energy redox dyes. *Nature Photon.* **3**, 406–411 (2009).
- 29 14. Kuang, D. *et al.* Co-sensitization of organic dyes for efficient ionic liquid  
30 electrolyte-based dye-sensitized solar cells. *Langmuir* **23**, 10906–10909 (2007).
- 31 15. Yum, J. H., Baranoff, E., Wenger, S., Nazeeruddin, M. K. & Grätzel, M.  
32 Panchromatic engineering for dye-sensitized solar cells. *Energy Environ.  
Sci.* **4**, 842–857 (2011).
- 33 16. Jeong, N. C. *et al.* Effective panchromatic sensitization of electrochemical solar  
34 cells: strategy and organizational rules for spatial separation of complementary  
35 light harvesters on high-area photoelectrodes. *J. Am. Chem. Soc.* **134**,  
36 19820–19827 (2012).
- 37 17. Shrestha, M. *et al.* Dual functionality of BODIPY chromophore in porphyrin-  
38 sensitized nanocrystalline solar cells. *J. Phys. Chem. C* **116**, 10451–10460 (2012).
- 39 18. Nattestad, A. *et al.* Highly efficient photocathodes for dye-sensitized tandem  
40 solar cells. *Nature Mater.* **9**, 31–35 (2010).
- 41 19. Yamaguchi, T., Uchida, Y., Agatsuma, S. & Arakawa, H. Series-connected  
42 tandem dye-sensitized solar cell for improving efficiency to more than 10%.  
43 *Sol. Energy Mater. Sol. Cells* **93**, 733–736 (2009).
- 44 20. Murayama, M. & Mori, T. Dye-sensitized solar cell using novel tandem cell  
45 structure. *J. Phys. D* **40**, 1664–1668 (2007).
- 46 21. Kubo, W., Sakamoto, S., Kitamura, T., Wada, Y. & Yanagida, S. Dye-sensitized  
47 solar cells: improvement of spectral response by tandem structure. *J. Photochem.  
Photobiol. A* **164**, 33–39 (2004).
- 48 22. Ito, S. *et al.* Fabrication of thin film dye sensitized solar cells with solar to electric  
49 power conversion efficiency over 10%. *Thin Solid Films* **516**, 4613–4619 (2008).
- 50 23. Imahori, H., Umeyama, T. & Ito, S. Large π-aromatic molecules as potential  
51 sensitizers for highly efficient dye-sensitized solar cells. *Acc. Chem. Res.* **42**,  
52 1809–1818 (2009).
- 53 24. Bessho, T., Zakeeruddin, S. M., Yeh, C. Y., Diau, E. W. G. & Grätzel, M. Donor-  
54 acceptor-substituted porphyrins. *Angew. Chem. Int. Ed.* **49**, 6646–6649 (2010).
- 55 25. Chang, Y. C. *et al.* A strategy to design highly efficient porphyrin sensitizers for  
56 dye-sensitized solar cells. *Chem. Commun.* **47**, 8910–8912 (2011).
- 57 26. Hsieh, C. P. *et al.* Synthesis and characterization of porphyrin sensitizers with  
58 various electron-donating substituents for highly efficient dye-sensitized solar  
59 cells. *J. Mater. Chem.* **20**, 1127–1134 (2010).
- 60 27. Wu, S. L. *et al.* Design and characterization of porphyrin sensitizers with a push-  
61 pull framework for highly efficient dye-sensitized solar cells. *Energy Environ. Sci.* **3**,  
62 949–955 (2010).
- 63 28. Lee, C. W. *et al.* Novel zinc porphyrin sensitizers for dye-sensitized solar cells:  
64 synthesis and spectral, electrochemical, and photovoltaic properties. *Chem.  
Eur. J.* **15**, 1403–1412 (2009).
- 65 29. Wang, C. L. *et al.* Enveloping porphyrins for efficient dye-sensitized solar cells.  
66 *Energy Environ. Sci.* **5**, 6933–6940 (2012).
- 67 30. Mathew, S. *et al.* Optical, electrochemical, and photovoltaic effects of an  
68 electron-withdrawing tetrafluorophenylene bridge in a push–pull porphyrin  
69 sensitizer used for dye-sensitized solar cells. *J. Phys. Chem. C* **115**,  
70 14415–14424 (2011).
- 71 31. Zhou, W. *et al.* Porphyrins modified with a low-band-gap chromophore for dye-  
72 sensitized solar cells. *Org. Electron.* **13**, 560–569 (2012).
- 73 32. Susumu, K., Duncan, T. V. & Therien, M. J. Potentiometric, electronic structural,  
74 and ground- and excited-state optical properties of conjugated  
75 bis[(porphinato)zinc(II)] compounds featuring proquinoidal spacer units.  
76 *J. Am. Chem. Soc.* **127**, 5186–5195 (2005).
- 77 33. Song, H. J., Kim, D. H., Lee, T. H. & Moon, D. K. Emission color tuning of  
78 copolymers containing polyfluorene, benzothiadiazole, porphyrin derivatives.  
79 *Eur. Polym. J.* **48**, 1485–1494 (2012).
- 80 34. Lash, T. D., Chandrasekar, P., Osuna, A. T., Chaney, S. T. & Spence, J. D.  
81 Porphyrins with exocyclic rings. 13. synthesis and spectroscopic characterization  
82 of highly modified porphyrin chromophores with fused acenaphthylene and  
83 benzothiadiazole rings. *J. Org. Chem.* **63**, 8455–8469 (1998).
- 84 35. Huang, Y., Li, L., Peng, X., Peng, J. & Cao, Y. Solution processed small molecule  
85 bulk heterojunction organic photovoltaics based on a conjugated donor–  
86 acceptor porphyrin. *J. Mater. Chem.* **22**, 21841–21844 (2012).
- 87 36. Gao, P. *et al.* Facile synthesis of bulky BPTPA donor group suitable for cobalt  
88 electrolyte based dye sensitized solar cells. *J. Mater. Chem. A* **1**, 5535–5544  
89 (2013).
- 90 37. Kasha, M., Rawls, H. R. & El-Bayoumi, M. A. The exciton model in molecular  
91 spectroscopy. *Pure Appl. Chem.* **11**, 371–392 (1965).
- 92 38. Gouterman, M. Study of the effects of substitution on the absorption spectra of  
93 porphyrin. *J. Chem. Phys.* **30**, 1139–1161 (1959).
- 94 39. Gouterman, M. Spectra of porphyrins. *J. Mol. Spectrosc.* **6**, 138–163 (1961).
- 95 40. Zhao, Y. & Truhlar, D. G. The M06 suite of density functionals for main group  
96 thermochemistry, thermochemical kinetics, noncovalent interactions, excited  
97 states, and transition elements: two new functionals and systematic testing of  
98 four M06-class functionals and 12 other functionals. *Theor. Chem. Acc.* **120**,  
99 215–241 (2008).
- 100 41. Duffy, N. W., Dobson, K. D., Gordon, K. C., Robinson, B. H. & McQuillan, A. J.  
101 *In situ* infrared spectroscopic analysis of the adsorption of ruthenium (II)  
102 bipyridyl dicarboxylic acid photosensitisers to TiO<sub>2</sub> in aqueous solutions. *Chem.  
Phys. Lett.* **266**, 451–455 (1997).
- 103 42. Jones, F., Farrow, J. B. & van Bronswijk, W. An infrared study of a polyacrylate  
104 flocculant adsorbed on hematite. *Langmuir* **14**, 6512–6517 (1998).
- 105 43. Kira, A. *et al.* Effects of π-elongation and the fused position of quinoxaline-fused  
106 porphyrins as sensitizers in dye-sensitized solar cells on optical, electrochemical  
107 and photovoltaic properties. *J. Phys. Chem. C* **114**, 11293–11304 (2010).
- 108 44. Longhi, E. *et al.* Metal-free benzothiadiazole-containing organic dyes for dye-  
109 sensitized solar cells. *Eur. J. Org. Chem.* **2013**, 84–94 (2013).
- 110 45. Haid, S. *et al.* Significant improvement of dye-sensitized solar cell performance  
111 by small structural modification in π-conjugated donor–acceptor dyes. *Adv.  
Funct. Mater.* **22**, 1291–1302 (2012).
- 112 46. Barnes, P. R. F. *et al.* Interpretation of optoelectronic transient and charge  
113 extraction measurements in dye-sensitized solar cells. *Adv. Mater.* **25**,  
114 1881–1922 (2013).
- 115 47. O'Regan, B. C. & Lenzmann, F. Charge transport and recombination in a  
116 nanoscale interpenetrating network of n-type semiconductors: transient  
117 photocurrent and photovoltage studies of TiO<sub>2</sub>/dye/CuSCN photovoltaic cells.  
118 *J. Phys. Chem. B* **108**, 4342–4350 (2004).
- 119 48. O'Regan, B. C. *et al.* Measuring charge transport from transient photovoltage  
120 rise times: a new tool to investigate electron transport in nanoparticle films.  
121 *J. Phys. Chem. B* **110**, 17155–17160 (2006).
- 122 49. Acknowledgements (127)
- 123 The research leading to these results received funding from Solvay Fluor GmbH, the  
124 European Union Seventh Framework Programme (FP7/2007–2013) under grant agreement  
125 ‘ENERGY-261920, ESCORT’ and SSSTC (Sino-Swiss Science and Technology  
126 Cooperation), and the European Community’s Seventh Framework Programme (FP7/2007–  
127 2013) under grant agreement no. 246124 of the SANS project. M.G. thanks the European  
128 Research Council (ERC) for supporting part of this work under the advanced research grant  
129 (no. 247404) MESOLIGHT. A.Y. acknowledges the Balzan Foundation for support as part of  
130 the Balzan prize awarded to M.G. in 2009. M.K.N. acknowledges the World Class University  
131 programme, Photovoltaic Materials, Department of Material Chemistry, Korea University,  
132 Chungnam, 339–700, Korea, funded by the Ministry of Education, Science and Technology  
133 through the National Research Foundation of Korea (no. R31-2008-000-10035-0).  
134
- 135 50. Author contributions (139)
- 136 A.Y. and S.M. proposed the research. S.M. synthesized and characterized the dyes with  
137 assistance from P.G. A.Y. fabricated and optimized the DSCs and conducted all the  
138 photovoltaic characterization. Electrochemical characterization was performed by P.G.  
139 R.H.B performed photo-physical characterization and assisted in interpreting the results  
140 with assistance from A.Y. and M.G. R.H.B designed the instruments and contributed to  
141 interpreting the results. B.F.E.C. and N.A.A. performed the computational characterization,  
142 with I.T. and U.R. contributing to the analysis and interpretation of the results. M.K.N. is  
143 responsible for overseeing the sensitizer project. S.M. and M.G. prepared the manuscript,  
144 with invaluable contributions from A.Y., R.H.B., M.K.N., B.F.E.C., N.A.A., I.T. and U.R.  
145
- 146 51. Additional information (149)
- 147 Supplementary information and chemical information are available in the online version of  
148 the paper. Reprints and permissions information is available online at www.nature.com/  
149 reprints. Correspondence and requests for materials should be addressed to M.K.N. and M.G.  
150
- 151 52. Competing financial interests (153)
- 152 The authors declare no competing financial interests.  
153

Publisher: Nature

Journal: Nature Chemistry

Article number: nchem.1861

Author (s): Mathew *et al.*

Title of paper: Dye-sensitized solar cells with 13% efficiency achieved through the molecular engineering of porphyrin sensitizers

**Please check that insertion of mention of Figure 3 is OK as added**

Query no.	Query	Response
1	Please check that sentence beginning “The development” is OK as amended	
2	Sentence beginning “The presence” OK as amended?	
3	HOMO expanded OK?	
4	LUMO expanded OK?	
5	FTIR expanded OK?	
6	Sentence beginning “Interestingly” OK as amended? Should we be referring to plural “electrons”?	
7	Please expand IPCE	
8	Ref 38 – please check article title	
9	Please check that Table 1 is OK as amended	
10	Please check that insertion of mention of Figure 3 is OK .	